Final Report of AFSR-AOARD Project AOARD-07-4098

"Study of Equatorial Ionospheric Irregularities with ROCSAT-1/IPEI Data for Assessment of Impacts on Communication/Navigation System (IV)"

PI C. H. Liu

Co PI S.-Y. Su

National Central University, Taiwan, R. O. C.

September 1, 2008

Report Documentation Page

Form Approved
OMB No. 0704-0188

1. REPORT DATE	2. REPORT TYPE	3. DATES COVERED
23 OCT 2008	**FInal**	**18-09-2007 to 17-09-2008**

4. TITLE AND SUBTITLE
Study of Equatorial Ionospheric Irregularities with ROCSAT- 1/IPEI Data for Assessment of Impacts on

5a. CONTRACT NUMBER
FA48690714098

5b. GRANT NUMBER

5c. PROGRAM ELEMENT NUMBER

6. AUTHOR(S)
Chao-Han Liu

5d. PROJECT NUMBER

5e. TASK NUMBER

5f. WORK UNIT NUMBER

7. PERFORMING ORGANIZATION NAME(S) AND ADDRESS(ES)
National Central University,Institute of Space Science,Chung-Li 320, Taiwan,Taiwan,TW,320

8. PERFORMING ORGANIZATION REPORT NUMBER
N/A

9. SPONSORING/MONITORING AGENCY NAME(S) AND ADDRESS(ES)
AOARD, UNIT 45002, APO, AP, 96337-5002

10. SPONSOR/MONITOR'S ACRONYM(S)
AOARD

11. SPONSOR/MONITOR'S REPORT NUMBER(S)
AOARD-074098

12. DISTRIBUTION/AVAILABILITY STATEMENT
Approved for public release; distribution unlimited

13. SUPPLEMENTARY NOTES

14. ABSTRACT
(1) Study the Cause of Seasonal/Longitudinal(s/l) Variations of Equatorial Irregularity Occurrences: The examination of global monthly occurrence pattern of density irregularities indicates that a smooth and slow variation in the occurrence pattern exists from one longitude sector to the next. Such variation should be related to the smooth and slow variations of the magnetic declination as well as the longitudinal variation of the geographic location of the dip equator for the ionospheric property. The effects of the magnetic declination and the ionospheric condition initially affect the s/l distribution of the post-sunset vertical drift velocities that then result in the same s/l variations of the irregularity occurrences. Thus, other factors such as the seed distribution for the instability perturbation from the atmospheric disturbance probably play no role in determining the s/l variations of irregularity occurrences. (2) Initial Result of Seasonal/Longitudinal (s/l) Distribution of Irregularity Spectra Indices There is some argument of identifying the outer-scale length of the irregularity turbulence correctly to obtain the turbulence strength parameter Cs. However, this will be cleared in the upcoming project when a coincident event between the ROCSAT and scintillation experiment at Ascension Island is studied in the later part of 2008. (3) Management of NCU-SCINDA Station and Study the Coincident Observation Events with FORMOSAT-3/COSMIC and C/NOFS The NCU-SCINDA Station is being managed smoothly with continuous operation up to now. All the full-wave mode (100 Hz) data during the nighttime have been collected so far.

15. SUBJECT TERMS
Atmospheric Chemistry, Atmospheric Science, Ionospheric Irregularities

16. SECURITY CLASSIFICATION OF:			17. LIMITATION OF ABSTRACT	18. NUMBER OF PAGES	19a. NAME OF RESPONSIBLE PERSON
a. REPORT	b. ABSTRACT	c. THIS PAGE			
unclassified	**unclassified**	**unclassified**	**Same as Report (SAR)**	**23**	

Summary of Final Report

Completed and Delivered Items:

(1) Study the Cause of Seasonal/Longitudinal (s/l) Variations of Equatorial Irregularity Occurrences. (Published in Journal of Geophysical Research-Space Physics, May 31, 2008)

This study started from the last project period (AOARD-06-4046), and is now completed and published in May, 2008 in Journal of Geophysical Research- Space Physics (complete paper is attached in Appendix I). The examination of global monthly occurrence pattern of density irregularities indicates that a smooth and slow variation in the occurrence pattern exists from one longitude sector to the next. Such variation should be related to the smooth and slow variations of the magnetic declination as well as the longitudinal variation of the geographic location of the dip equator for the ionospheric property. The effects of the magnetic declination and the ionospheric condition initially affect the s/l distribution of the post-sunset vertical drift velocities that then result in the same s/l variations of the irregularity occurrences. Thus, other factors such as the seed distribution for the instability perturbation from the atmospheric disturbance probably play no role in determining the s/l variations of irregularity occurrences.

(2) Initial Result of Seasonal/Longitudinal (s/l) Distribution of Irregularity Spectra Indices.

We have been using the 32-Hz ROCSAT density data to obtain the s/l distributions of the irregularity spectra variation. First, the s/l distributions of irregularity spectra slope between 1 km and 7.6 km in the scale-length is obtained. The spectra slopes are then used to obtain the turbulence strength parameter C_s. Then the scintillation index S4 is calculated as shown in one example of Figure 1. Data in 2000 have been studied and a global scintillation model is being constructed. There is some argument of identifying the outer-scale length of the irregularity turbulence correctly to obtain the turbulence strength parameter C_s. However, this will be cleared in the upcoming project when a coincident event between the ROCSAT and scintillation experiment at Ascension Island is studied in the later part of 2008.

(3) Management of NCU-SCINDA Station and Study the Coincident Observation Events with FORMOSAT-3/COSMIC and C/NOFS. (Continuing)

The NCU-SCINDA Station is being managed smoothly with continuous operation up to now. All the full-wave mode (100 Hz) data during the nighttime

have been collected so far. In May 2008, Dr. S. Tulasi Ram, a PostDoc of PI, Prof. C. H. Liu joined the project to study the full-wave mode data. We have found that the data received by the 2 antennas separated by 75 meters could not be used to derive the drift velocity of the irregularity structure as noted in Figure 2. The cause of failure is still under investigation. However, it seems to be caused by the hardware failure. Furthermore, noise contamination is found in all the data up to July 2007 as shown in Figure 3. Fortunately, data after July 2007 is good and reveals scintillation occurrences when they appear. We will use these good data to study the coincident observations with FORMOSAT-3/COSMIC, and with C/NOFS in 2008-2009.

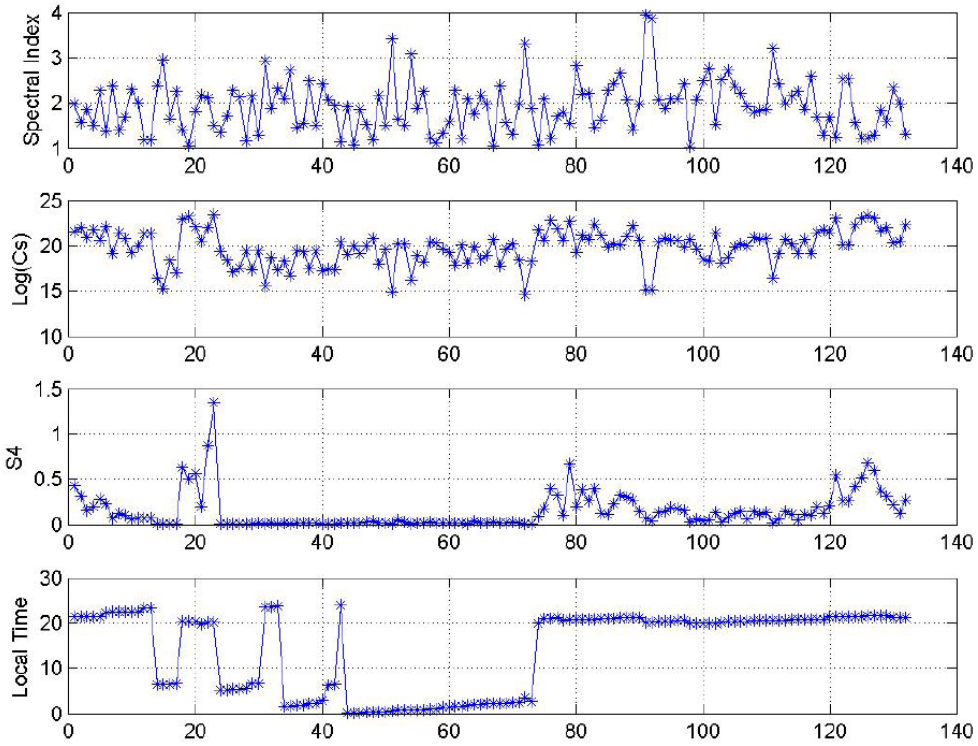

Fig. 1. Study of scintillation index S_4 derived from density irregularities observed by ROCSAT-1. Panels from top to bottom are the variations of the spectral index in the density power spectra of the irregularity structure, the derived turbulence strength parameter, the resultant scintillation index S_4 for 1.2 GHz radio wave, and the local time distribution of the occurrences, respectively.

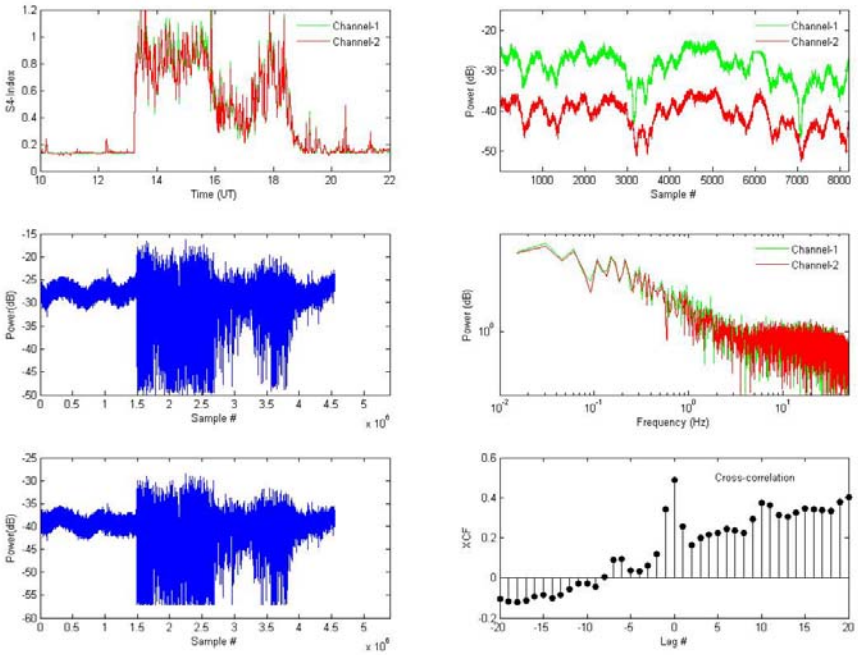

Fig. 2. Example of cross-correlation study of signals from channels 1 and 2 to obtain the drift of the irregularity intercepted by the NCU-SCINDA station. Although the signals look good, the result of cross-correlation (shown in the last panel in the bottom right-hand side) indicates that no drift of the irregularity structure can be obtained because the peak of the cross-correlation is located at the zero time-lag.

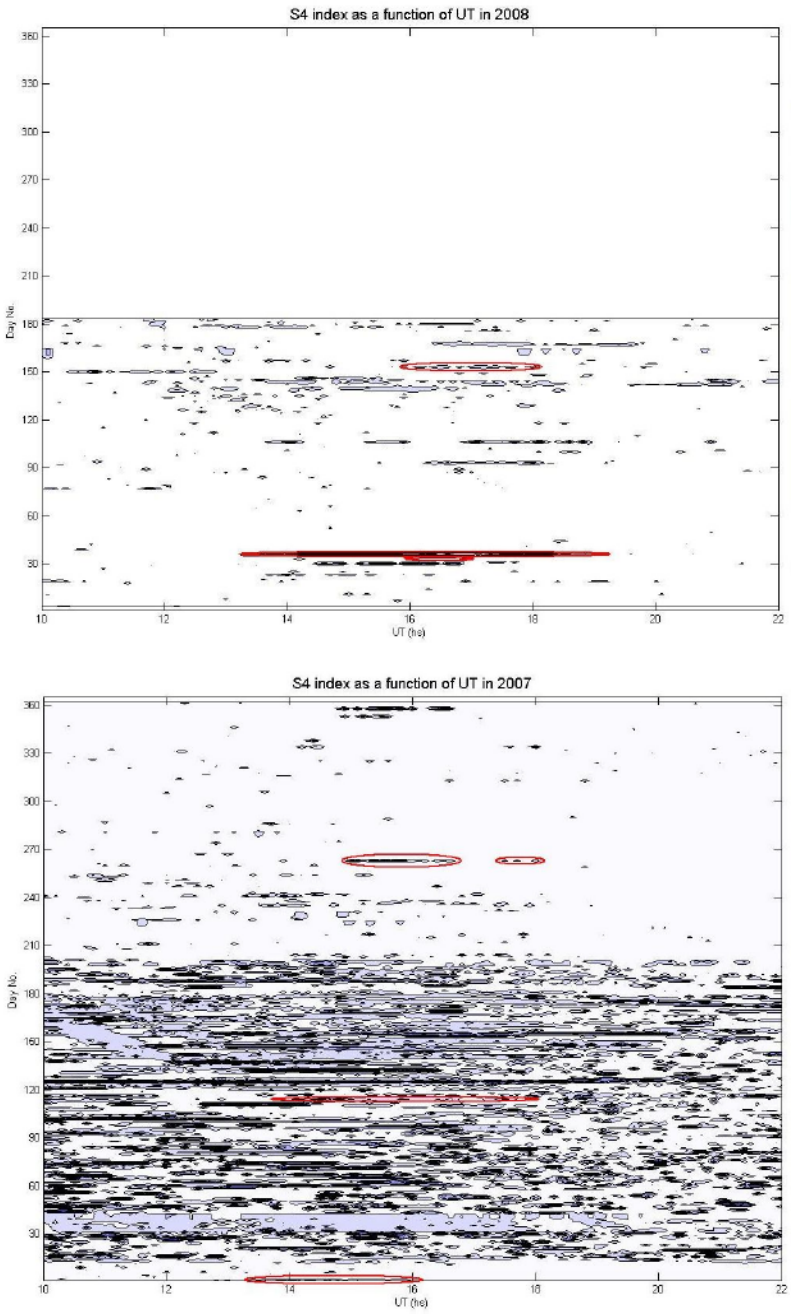

Fig. 3. The chronology of the occurrences of scintillation index S_4 observed by NCU-SCINDA station in 2007 and 2008. Notice the contamination of signals in 2007 stops on day 200. After that day, the noise disappears and good scintillation event has been noted.

Appendix I

JOURNAL OF GEOPHYSICAL RESEARCH, VOL. 113, A05307, doi:10.1029/2007JA012809, 2008

On monthly/seasonal/longitudinal variations of equatorial irregularity occurrences and their relationship with the postsunset vertical drift velocities

S.-Y. Su,[1] C. K. Chao,[2] and C. H. Liu[3]

Received 10 September 2007; revised 19 November 2007; accepted 14 January 2008; published 16 May 2008.

[1] Monthly variation of global equatorial density irregularity distribution has been obtained with the data taken by ROCSAT-1 at the 600 km topside ionosphere from March 1999 to June 2004 during high to moderate solar activity years. This global distribution of monthly irregularity occurrence rate not only provides the best spatial/temporal distribution in existence so far but also serves to fill the gap of irregularity distribution missing over some eastern Pacific region where no ground observation is available. The 5 1/2-year result of the monthly occurrence pattern indicates a smooth variation across the longitudes contrary to some beliefs that a drastic change in irregularity occurrence pattern has occurred across the eastern Pacific longitudes. Excellent agreement is noted for the current results with Aarons' (1993) conjectured sketch of the global scintillation distribution. Furthermore, the seasonal/longitudinal (s/l) variations of quiet time postsunset vertical drift velocities are found to track closely with the s/l variations of irregularity occurrences. Linear regression analysis between the vertical drift velocity and the irregularity occurrence rate indicates that the vertical drift velocities at three different longitude zones of magnetic declination have good correlations with the irregularity occurrences for all seasons. This implies that the averaged postsunset vertical drift velocity is a good indicator for the occurrences of equatorial density irregularities in a longitude region of similar magnetic declination. The smooth variation of monthly/seasonal/longitudinal distributions of the vertical drift velocities that results in the smooth variation of topside density irregularity occurrences implies that the global occurrence pattern of either distribution is controlled by the smooth global variation of the postsunset ionospheric condition, related to the magnetic declination effect and the seasonal variation of the ionospheric density level at the dip equator located with respect to the geographic equator. There seems little need to include the global distribution of instability perturbation seeds from atmospheric disturbances to complete the global distribution of topside irregularity occurrences.

Citation: Su, S.-Y., C. K. Chao, and C. H. Liu (2008), On monthly/seasonal/longitudinal variations of equatorial irregularity occurrences and their relationship with the postsunset vertical drift velocities, *J. Geophys. Res.*, *113*, A05307, doi:10.1029/2007JA012809.

1. Introduction

[2] Global seasonal/longitudinal (s/l) distributions of ionospheric irregularities have been studied with ground and space observations in the past [*Basu et al.*, 1976; *Aarons*, 1977, 1982, 1993; *Maruyama and Matuura*, 1980, 1984; *Tsunoda*, 1985; *Watanabe and Oya*, 1986; *Kil and Heelis*, 1998; *McClure et al.*, 1998; *Huang et al.*, 2002; *Hei et al.*, 2005; *Su et al.*, 2006]. However, because of satellite's short lifetime in operation, many space observations seldom provide a long record of data to study the monthly variation of irregularity occurrences at one particular longitude region. Long records of fine temporal resolution in the monthly irregularity occurrence variation at one longitude region is usually provided by a ground observation with radar, ionosonde, or scintillation data [e.g., *Aarons*, 1982, 1993; *Bowman*, 1984; *Tsunoda*, 1985; *Abdu et al.*, 1981, 1992]. Since there are not enough ground stations to cover the whole globe, the longitudinal distribution of monthly irregularity occurrences with good temporal resolution has not been documented yet. In particular, there is no ground observation available at longitudes from 180 to 280° in the eastern Pacific region [*Basu and Basu*, 1985]. This data gap seems to lead some speculation that an abrupt

[1] Institute of Space Science and Center for Space and Remote Sensing Research, National Central University, Chung-Li, Taiwan.
[2] Institute of Space Science, National Central University, Chung-Li, Taiwan.
[3] Academia Sinica, Taipei, Taiwan.

0148-0227/08/2007JA012809$09.00

change in the monthly occurrence pattern across these longitudes has occurred because the data from either side of this longitude region indicates different monthly occurrence patterns. Although there is a large change in the topological feature from the eastern Pacific to the South American continent to imply that different instability condition could have existed to affect the irregularity occurrence processes, it is uncertain if such a process has ever resulted in different monthly occurrence pattern in the data gap region.

[3] ROCSAT-1 satellite, orbiting at 600 km altitude with 35° inclination, was in mission from March 1999 through June 2004 around the solar max period of solar cycle 23. The onboard ionospheric and plasma electrodynamics instrument (IPEI) operates at 100% duty cycle to take continuous data of ion density, flow velocity, temperature, and ion composition in the low-to-middle latitude ionosphere throughout the 5 1/2-year lifetime. This data set constitutes the best data set of the topside ionospheric observations at low-to-middle latitudes since the ends of the U.S. Atmospheric Explorer E (AE-E) mission in 1981 [e.g., *McClure et al.*, 1998; *Kil and Heelis*, 1998] and the Japanese Hinotori mission in 1982 [e.g., *Watanabe and Oya*, 1986]. There are other short-lived low-latitude ionospheric observation missions such as the San Marco mission that did not provide enough data to construct a statistical model. The long operated Defense Meteorological Satellite Program (DMSP) has been collecting data for more than a decade but the mission has only covered some specific local time regions [*Huang et al.*, 2002]. Similarly, the s/l distributions of equatorial spread-*F* events observed by the polar-orbiting CHAMP satellite between 380 and 450 km altitudes from 2001 to 2004 cannot provide fine spatial/temporal resolution as the low-latitude-orbiting ROCSAT does [*Stolle et al.*, 2006]. Only the scheduled C/NOFS (Communication/Navigation Outage Forecasting System) mission could probably provide data that exceed the ROCSAT/IPEI data in quality, quantity and significance for the low-latitude ionospheric study. However, C/NOFS is scheduled to launch in April of 2008 and operates in the beginning years of solar cycle 24 when the solar activity is low. Thus the ROCSAT/IPEI data set still remains the best data set to study the equatorial electrodynamics during high solar activity periods. The constructed global distribution of monthly irregularity occurrence pattern will be valuable for comparison with the ground observation at any longitude. This is especially true in the eastern Pacific region where no ground observation is available so far.

[4] In addition, as the postsunset ionospheric height has been attributed as one of the most important factors for the occurrence of equatorial irregularity [e.g., *Farley et al.*, 1970; *Ossakow et al.*, 1979; *Rastogi*, 1980; *Abdu et al.*, 1983; *Sultan*, 1996; *Fejer et al.*, 1999], the ROCSAT observed quiet time postsunset vertical drift velocities will also be used to study the background ionospheric condition in relation to the irregularity occurrences in the monthly/seasonal/longitudinal distributions. This is to see if an ionosphere that has been frequently observed to have a large postsunset vertical drift velocity will also has a high probability of observing density irregularities at a longitude region in every season.

2. ROCSAT/IPEI Observations

2.1. Quiet Time Monthly/Longitudinal Variations of Equatorial Irregularities

[5] Study of the seasonal/longitudinal (s/l) distributions of topside ionospheric irregularity occurrences at low-to-middle latitudes with the ROCSAT/IPEI data has been published before [*Su et al.*, 2006]. Here we use the same data set to construct a detailed global monthly variation of equatorial irregularity occurrences within ±15° in dip latitude during magnetic quiet times ($K_p < 3$). Because the 5 1/2-year data is taken during moderate to high solar activity years, the solar activity effect on the equatorial irregularity occurrences is also studied with the distribution taken during a high solar activity year of 2000 against the distribution in a moderate solar activity year of 2003. All these results are shown in Figure 1. The global monthly occurrence variation is shown in 36 longitude sectors (sections). In each longitude sector, the solid line represents the 5 1/2-year averages of the occurrence rate, while the dashed line is for year 2000 and the dotted line, for year 2003.

[6] We use the first letter of the month to represent the month in a year in the horizontal axis of each section in Figure 1, such as J for January, F for February, and so on. Then a season of the March equinox will include FMA months; June solstice has MJJ months; September equinox has ASO months; and December solstice has NDJ months. As we start to inspect each section in Figure 1 for the global longitudinal variation of the 5 1/2-year averaged irregularity occurrence rate (shown in solid lines), we notice that at longitudes 0–10° shown in the upper-left section of Figure 1, the monthly occurrence peaks in both equinox seasons and has a minimum during the December solstices. A valley in the monthly occurrence pattern is noted in the June solstice. This monthly occurrence pattern remains very similar to each other from one longitude sector to the next except that the peaks and valley change slowly, as we move eastward until we arrive at longitudes 50–60°. In this region, the valley becomes so low that the months for the minimum occurrence rates now include the June solstice in addition to the December solstice. Similar feature of double peaks of high occurrences in both equinoxes and double dips of low occurrences in two solstices is maintained for a longitudinal span of about 100° until the longitude sector of 140–150° is reached. From here on, the low occurrence rate during the June solstice gradually increases until it attains a maximum at the longitude sector of 160–170°. On the other hand, the December solstice months still retain the minimum occurrence rates. Moving further eastward, the months of the maximum occurrence begin to shift toward the September equinox. As the occurrence rates in the June solstice begin to decrease at the longitude sector of 210–220°, a small peak in the March equinox reappears as we move further eastward until the occurrence rates in the June solstice become the minimum at longitudes 230–240°. At this longitude sector, the occurrence maxima return to the two equinoxes. From here on, the minimum occurrence rate stays in the June solstice and the occurrence rates during the

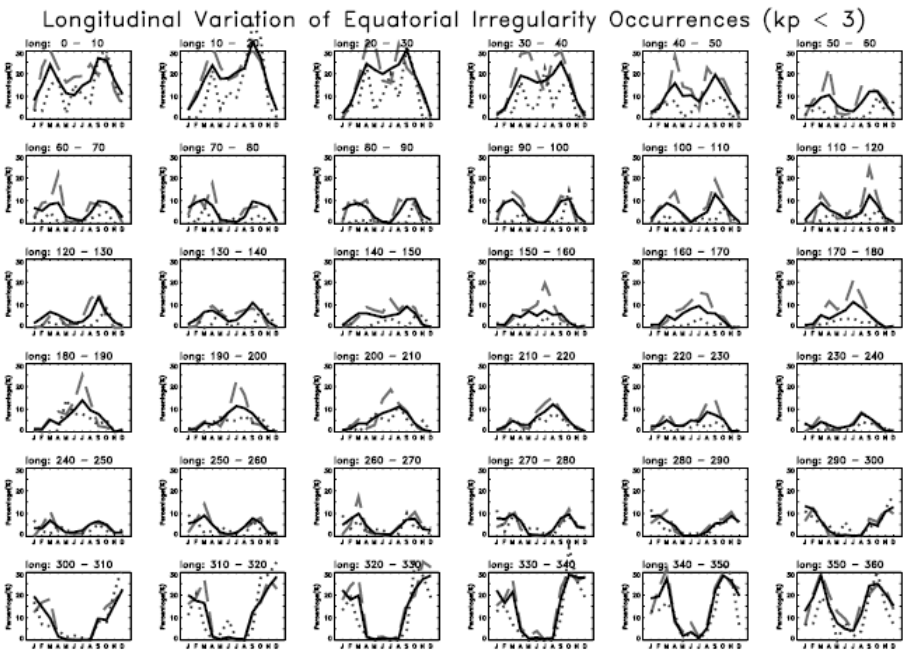

Figure 1. Monthly variation of global longitudinal distribution of topside equatorial irregularity occurrences observed by ROCSAT-1 from 1999 to 2004.

December solstice begin to peak and overtake the two equinoctial peaks to become the maximum at longitudes 280–290°. The maximum occurrence rate during the December solstice remains very high and the minimum stays in the June solstice until we reach the longitude sector 340–350°, where the maximum rate during the December solstice begins to subside and two peaks in the two equinoxes become apparent as we move eastward to return to the prime meridian to complete the inspection of the global variation in Figure 1.

[7] Inspection of Figure 1 leads us to realize that the gross feature of the monthly irregularity occurrence pattern changes slowly and smoothly across the longitudes. There is no large or abrupt pattern change from one longitude sector to the next. The maximum occurrence rate in a particular month at one longitude will change to become the minimum in the same month at a different longitude sector, but the change is gradual across the longitudes. For example, a maximum occurrence rate at the longitude sectors from 160 to 200° is noticed during the June solstice. The maximum then becomes the minimum in the same solstice season if we move a third way across the globe to the longitude sectors 290–330°. Opposite case in the occurrence rate change is also noticed in the same two longitude sectors during the December solstice. However, any large pattern change between two different longitude sectors for the same month (season) is accomplished with a smooth and gradual change in the occurrence pattern across the longitudes between the two.

[8] Thus as we examine Figure 1 for the monthly variation of irregularity occurrences for the locations across the longitudes from 180 to 280° in the eastern Pacific region where no ground observation is available so far, we notice that two different monthly occurrence patterns existed during the June solstice outside this region. One pattern indicates that a maximum occurrence rate in July is observed at longitudes from 160 to 170°. The peak occurrence rate then increases and shifts toward the September equinox as we move eastward. At longitudes 230–240°, a minimum occurrence rate then appears during May, the beginning of June solstice months. This minimum occurrence rate then extends to cover the whole June solstice months as we move further eastward to the longitudes 270–280°, where the minimum occurrence rate dips to near-zero in the June solstice. This minimum near-zero occurrence rate in the June solstice is maintained up to the longitudes 290–340°, where a dominant and prevailing maximum appears during the December solstice. Thus without the current ROCSAT observation to fill the gap for the longitude sectors between 180 and 280°, one could be misled by the existing ground observations that a monthly maximum occurs in July at the longitude sector 160–170°, but drops to minimum

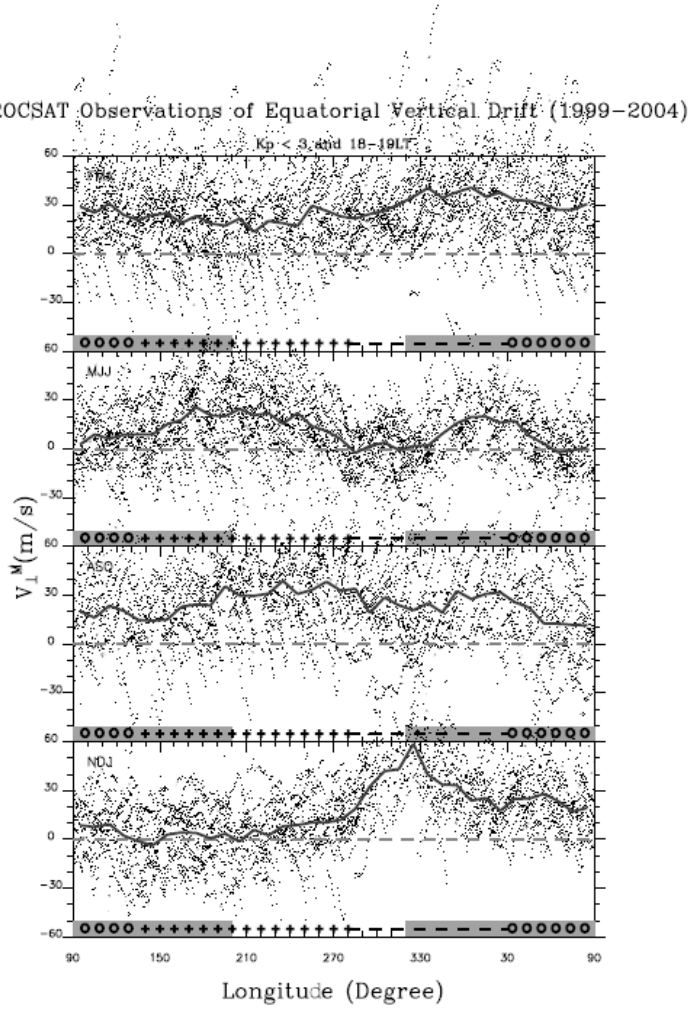

Figure 2. Seasonal/longitudinal distributions of equatorial vertical drift velocities observed by ROCSAT-1 in 18–19 h local time (LT) sector during quiet magnetic periods with no irregularity occurrences during each equatorial crossing. Shaded and unshaded bar regions indicate the location of the dip equator in the Northern and Southern Hemisphere, respectively. The plus, minus, and circle signs indicate the longitude zones of positive, negative, and near-zero magnetic declination, respectively, at the dip equator.

during the June solstice at the longitude sector 290–340° and concludes that an abrupt change in the monthly occurrence variation exists between 180 and 280°. An abrupt change indeed, but the change is, in fact, gradual across some large longitude sectors over the eastern Pacific.

[9] The final note in Figure 1 is to compare the results observed during the high solar activity year of 2000 (drawn in dashed lines) with that in the moderate active year of 2003 (in dotted lines). Year 2000 is the solar maximum of cycle 23 with the yearly averaged $F_{10.7}$ of 180, while year 2003 is in the beginning of the decline phase with the yearly averaged $F_{10.7}$ of 130. The monthly average of $F_{10.7}$ in 2000 is always higher than that of 2003. Thus we notice that the monthly occurrence rate in 2000 is, for the most of the time,

higher than that in 2003; and the 5 1/2-year averages fall between the two. Such occurrence pattern is in agreement with past observations that the equatorial irregularity occurrence rate is, in general, correlated with solar activity. However, there is opposite occurrence pattern noticed for a higher monthly occurrence rate in 2003 at some longitude sectors. Such contrasting observation has been studied and reported in a separate paper [*Su et al.*, 2007]. Here in Figure 1, we only point out that the global longitudinal variation of monthly occurrence rate correlates with solar activity, in general.

2.2. Quiet Time Seasonal/Longitudinal Variations of the Postsunset Vertical Drift Velocities

[10] The vertical ion drift velocities measured by ROCSAT-1 in the equatorial region between ±5° of the dip equator are obtained during the magnetic quiet times ($K_p < 3$) and without equatorial irregularity activities during each equatorial crossing of the ROCSAT orbit. This constitutes an average equatorial vertical drift velocity distribution during a quiet period without geomagnetic as well as irregularity activity. In the current report, we present the s/l distributions of equatorial vertical drift velocities in the 18–19 h local time (LT) sector in Figure 2. The reason to select the vertical drift velocity in this local time sector is that the occurrence of equatorial density irregularities is known to start from the local sunset at around 18 h LT. Furthermore, the vertical drift velocities in the 18–19 h LT sector can adequately represent the rising velocities of the prereversal enhancement (PRE) that drives the postsunset ionosphere to a higher altitude to cause the occurrences of equatorial density irregularities. Therefore, the correlation study carried out in the later section between the vertical drift velocities at 18–19 h LT and the occurrence of equatorial density irregularities could shed light on the causal relationship between them.

[11] There are four sections in Figure 2 showing the longitudinal distributions of vertical drift velocities, from top to bottom, for the March equinox, the June solstice, the September equinox, and the December solstice season, respectively. In each section of a season, we show the scatters of the measured vertical drift velocities averaged from nine middle values in every 15 s (data points). The averaged vertical drift velocity within each 10° longitude bin is connected with a solid line to show the longitudinal variation in a season. The connected averaged vertical drift velocities indicate some uneven variation across the longitudes from statistical fluctuations due to low data points in a 10° longitude bin. However, the gross feature of the global variation in each season can still be recognized.

[12] The s/l distributions of the averaged vertical drift velocities shown in Figure 2 indicate that large longitudinal variations exist in two solstice seasons. There is a very low or near-zero averaged vertical drift velocity existed at certain longitudes during the solstice season in contrast to the smaller variation observed during the two equinoxes. Specifically, we found the near-zero vertical drift velocities at longitudes between 290 and 340° and between 60 and 90° during the June solstice. During the December solstice, the near-zero vertical drift velocities are observed at longitudes from 120 to 230°. This can be understood from the fact that large magnetic declinations, either positive or negative, exist at these longitude regions. To facilitate the explanation of observations, plus signs for the longitudes of positive magnetic declination from 140 to 280°, and minus signs for the longitudes of negative declination from 280° through the prime meridian to 30°, are added in the bottom of each section to indicate the magnetic declination at the dip equator in the longitude region of discussion. For longitude sectors at longitudes with small, near-zero magnetic declination from 30 to 140°, circle signs are used. The longitude sector from 60 to 90° could have belonged to the longitude zone of negative magnetic declination similar to that was done in the report of *McClure et al.* [1998], but we have put these longitudes into the longitude zone of near-zero magnetic declination to have three continuous zones of different magnetic declinations shown in Figure 2, instead. The shaded and unshaded bar regions in the bottom of each section indicate that the locations of the dip equator are in the Northern and Southern Hemisphere, respectively. It is noted that the longitudinal spans for the positive (plus signs) magnetic declinations in the shaded and in the unshaded zones are about the same. Similar width of longitudinal span for the negative (minus signs) magnetic declinations in the shaded against that in the unshaded zones is also noted. This is to point out that the magnetic declination effect from either positive (plus signs) or negative (minus signs) zone is about the same in either shaded (Northern Hemisphere) or unshaded zone (Southern Hemisphere).

[13] From the annotations in Figure 2, it is noted that the near-zero drift velocities are observed during the June solstice at longitudes 290–340° where the magnetic declinations are negative, and during the December solstice at longitudes 120–230° where the magnetic declinations are positive. As for the longitude region of 60–90° where magnetic declinations should have a small negative value even though it is classified into near-zero (circles) magnetic declination zone in Figure 2 for simplicity, a near zero drifts during the June solstice is in agreement with the observation made at longitudes 290–340°. The causes for these observations are all due to the so-called magnetic declination effect that will be discussed in section 3.3. The vertical drift velocities at these longitudinal regions further exhibit an anticorrelation property between the two solstice seasons. Again, this is correlated to the change of the magnetic declination effect during the respective opposite solstice season.

[14] Furthermore, in the longitude sectors of positive (plus signs) or negative (minus signs) magnetic declination zone, different trends in the vertical drift velocity variation in a solstice season are noticed. Specifically, during the June solstice, the vertical drift velocities increase in the positive (plus signs) zone from longitude 140 to 200°, but begin to decrease in the same positive zone from longitude 200 to 280°. This can be understood from the fact that the dip equator at longitudes 200–280° happens to locate in the Southern Hemisphere (indicated by the unshaded bar region in Figure 2) so that the local winter ionosphere condition of low density level in the June solstice fails to take the full advantage of the positive magnetic declination effect to have a large vertical drift velocity. Opposite behavior is also noted in the negative zones, where the vertical drift velocities indicate very small drift from longitude 280 to 320° but increases dramatically from 320 to 30°. This is due to local

summer effect in the ionospheric condition that exists at longitudes 320–30° to offset some of the negative magnetic declination effect. This will be further elaborated later in the discussion section 3.3. As for the December solstice, similar observations of contrasting variation trends in the vertical drift velocities are noticed between the longitudes 140–200° and 200–280° and between longitudes 280–320° and 320–30°. Again, this is due to local seasonal effect of the ionospheric condition in relation to the magnetic declination effect.

[15] As for the two equinox seasons, small longitudinal variations in the vertical drift velocities are noted. They vary between 15 and 40 m/s. However, the patterns of longitudinal variations in the vertical drift velocities for the two equinoxes are different from each other. The difference is manifested in the trend of longitudinal variation for having opposite low and high drift velocities appeared at longitudes from 150 to 280° in the March equinox and the September equinox, respectively. These longitudes indicate similar trends of opposite longitudinal variations in the vertical drift velocity pattern during the two solstice seasons. Since the magnetic declination effect is most noticed during a solstice season, some residual seasonal effect seems to be carried over to the following equinox season. Thus the high vertical drift velocities achieved at the positive magnetic declination zone at longitudes 140–280° during the June solstice are left to the following September equinox, and some of the low vertical drift velocities at the same zone observed during the December solstice are carried over to the following March equinox. A lesser degree of similar seasonal effect seems to exist at longitudes 280–30° where the magnetic declination is negative. Thus the effect of magnetic declination at the dip equator that seems to carry some residual seasonal effect to affect the vertical drift velocity.

3. Discussion

3.1. Longitudinal Distribution of Monthly Irregularity Occurrence Variations

[16] Before proceeding, we would like to mention that the density irregularities observed by ROCSAT at the 600 km altitude are related to the raised full-blown equatorial plasma bubble depletion structures. The growth and rise of these matured structures to the 600-km altitude is more related to the postsunset ionospheric condition that fosters the growth of instability process than to the perturbation seeds that initiate the instabilities [*Kil and Heelis*, 1998; *Su et al.*, 2006]. Therefore, the result of Figure 1 which indicates a smooth variation in the monthly occurrence pattern across two adjacent longitude sectors implies that the ionospheric condition varies smoothly across the longitudes. The ionospheric condition that favors the growth of equatorial Rayleigh-Taylor (R-T) instability process has been reported to come from two factors: (1) large zonal electric field resulted from the interaction of the eastward neutral wind with the ionosphere across the sunset terminator to raise the postsunset ionosphere high enough to accelerate the growth of the R-T instability process [*Rishbeth*, 1971, 1977, 1981; *Heelis et al.*, 1974; *Farley et al.*, 1970; *Zalesak and Ossakow*, 1980; *Ossakow*, 1981; *Abdu et al.*, 1982; *Batista et al.*, 1986; *Aarons*, 1993; *Fejer et al.*, 1999; G. Haerendel, unpublished report, 1974]; and (2) small meridional wind to reduce the hemispheric density distribution asymmetry to lessen the instability suppression effect [*Maruyama and Matuura*, 1984; *Maruyama*, 1988; *Sultan*, 1996; *Abdu et al.*, 2006; *Su et al.*, 2007]. Since the magnetic declination will affect the relative sunset times at conjugate *E* regions in factor 1 as well as the magnitude of the field-aligned transequatorial plasma flow in factor 2, it should play a dominant role in the growth of irregularity structures. As the magnetic declination varies smoothly across the longitudes, the resulting effect to influence the occurrence of equatorial irregularities in any month should also vary smoothly across the longitudes. Therefore, one should not expect a drastic change in the monthly occurrence pattern across the longitudes, and the result of Figure 1 clearly indicates so.

[17] In addition, hidden in factor 1 is the ionospheric density level that appears to affect the growth of irregularities during the June solstice at longitudes from 200 to 320° where the dip equator is located in the Southern Hemisphere, and during the December solstice at longitudes from 320 to 200° where the dip equator is located in the Northern Hemisphere with reference to the annotated information in Figure 2. The low density level during the June solstice apparently affects the growth of density irregularities even at the longitude regions from 230 to 280° where a positive magnetic declination exists to favor a high irregularity occurrence, yet the minimum irregularity occurrences appear instead as seen in Figure 1. This is termed "the local winter effect." This effect should first appear in the vertical drift velocities in these longitude regions then affects the occurrence of irregularities. This has been mentioned in section 2.2 and will be discussed further in section 3.3 where the cause of the vertical drift velocities is discussed. This minimum occurrence rate at longitudes 230–280° during the June solstice, in fact, has bridged a smooth variation across the longitudes between longitudes 120–180° and longitudes 310–340°, where a drastic contrast in irregularity occurrence pattern between the two regions exists. One pattern indicates that a maximum occurrence rate in July is observed at longitudes 160–170°, and the other, a near-zero minimum occurrence rate in the June solstice is seen at longitudes 270–340° with a dominant and prevailing maximum in the December solstice. The reason for the smooth bridge between two contrasting monthly occurrence variations in the two regions is caused by the local winter effect on the ionospheric density level at the longitudes 200–280° to decrease the July maximum gradually as we move across the longitude region that has the positive magnetic declination effect.

3.2. Comparison With Aarons' Sketch of Scintillation Occurrence Pattern

[18] In a review paper, *Aarons* [1993] indicates that as a function of longitude, "the morphology of *F*-region irregularities is vital for understanding the physics of the development of these irregularities." Utilizing then available scintillation data in conjunction with other in situ measurements, he has constructed an expected monthly occurrence variations of *F*-region scintillations (density irregularities) over many known ground stations. These stations are located at Huancayo, Peru at longitude −77°;

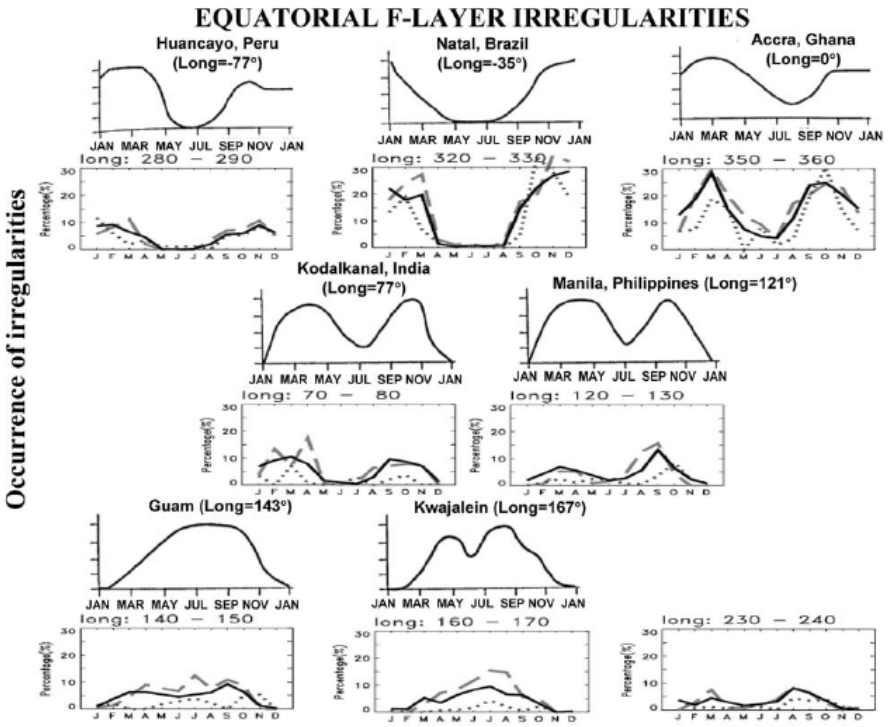

Figure 3. Comparison of *Aarons'* [1993] published monthly variations of scintillation occurrences over seven ground stations around the world (copied in the first, third, and fifth row from *Aarons* [1993] with kind permission of Springer Science and Business Media) with the ROCSAT observations of irregularity occurrence pattern (plotted in the second, fourth, and sixth row).

Natal, Brazil at longitude −35°; Accra, Ghana at longitude 0°; Kodaikanal, India at longitude 77°; Manila, Philippines at longitude 121°; Guam at longitude 143°, and Kwajalein at longitude 167°. The seven stations are distributed to separate by 50–70° in longitude between two adjacent stations except between Kwajalein and Huancayo where the longitudinal separation is 116°. There should be a station located around 220–240°, but unfortunately no such ground station existed in this Pacific region. The expected occurrence rate in each station is divided into four levels of scintillation activity to indicate the monthly occurrence variation. Aarons' results are copied in the first, third, and fifth row in Figure 3. In Figure 3, we copy the results from Figure 1 at the same longitude sectors of the seven stations and plotted them in the second, fourth, and sixth row for comparison. One extra observation at longitudes 230–240° from Figure 1 is added in the sixth row of Figure 3 to complete the global longitudinal distribution as observed by the ground stations.

[19] A simple inspection of Figure 3 will reveal the amazing resemblance of *Aarons'* [1993] expected monthly occurrence pattern in each station with the current ROCSAT result. The expected monthly occurrence pattern follows closely to the true averaged occurrence rate (in solid lines), except for one difference that is noted at Kwajalien where no dip in the occurrence rate is seen in the June solstice, but a high plateau is observed by ROCSAT instead. A small shift in the month for the minimum occurrence in the June solstice is also noticed at Accra in comparison with the ROCSAT data. All these differences could be caused by solar variability effect as we noticed how high solar activity (in dashed lines) and moderate solar activity (in dotted liens) can change the monthly occurrence variation slightly as seen in Figure 3.

[20] Comparing the original *Aarons'* [1993] results replotted in Figure 3 with the ROCSAT results again confirms our conclusion that the global longitudinal variation the monthly irregularity occurrences vary smoothly and

slowly across different ground stations within close longitudinal span. Since the ROCSAT results in Figure 3 show the true irregularity occurrence rates at these ground stations, it is hoped that the results (as well as the results in Figure 1) will be valuable for comparison with future scintillation experiments conducted at any station.

3.3. Causes of Seasonal/Longitudinal Variations of the Postsunset Vertical Drift Velocities

[21] The seasonal/longitudinal (s/l) distributions of vertical drift velocities shown in Figure 2 constitutes 1-h observation of the so-called prereversal enhancement (PRE) of the equatorial vertical drift velocities at 18–19 LT sector. So far, the global longitudinal variation of PRE has only been obtained from the observations with AE-E from 1977 to 1979 [*Fejer et al.*, 1995]. In that report, the local time variations of PRE at a few longitude sectors were emphasized. A more complete global variation of PRE using the same ROCSAT data has become available recently [*Fejer et al.*, 2008]. On the other hand, a model simulation result during an equinox season obtained from with MTIEGCM (Magnetospheric-Thermospheric-Ionospheric-Electrodynamics General Circulation Model) has been reported by *Vichare and Richmond* [2005]. Comparing the global variation of PRE peaks shown by of Vichare and Richmond in their Figure 3 with the result of the March equinox in Figure 2 of the current report, we notice that during high solar activity periods ($F_{10.7}$ = 200 in the simulation result), both results indicate very similar global longitudinal variation except that the simulated result has a peak PRE value of 80 m/s around longitude 300°, and a broad valley of 60 m/s between longitudes 180 and 240° that are about a factor of 2 to 4 higher than the March equinox values shown in Figure 2. The difference could be due to the fact that the ROCSAT observations are made at 600 km altitude in contrast to the simulated values taken at 300 km altitude. In addition, the ROCSAT measured vertical drift velocities are the averages at 18–19 LT sector, while the simulated values are for the peaks of PRE. Furthermore, as was mentioned before, the postsunset vertical drift velocities shown in Figure 2 indicate some differences in the s/l distributions between the March equinox and the September equinox. The observed September equinox value will then be different in the gross feature from the simulated equinox result of Vichare and Richmond. Different gross features in the global variations between the two equinoxes could exist but are not mentioned in their report.

[22] Since the cause of PRE has not been completely understood, it is hard to exactly explain the cause of the observed vertical drift velocities in Figure 2 as well as the cause for the different longitudinal variations in the two equinox seasons without a model simulation which is not available at the moment. However, from many theoretical simulation models published in the literature [e.g., *Batista et al.*, 1986; *Crain et al.*, 1993; *Eccles*, 1998a, 1998b; *Fesen et al.*, 2000; *Vichare and Richmond*, 2005], it is understood that the flux tube integrated Pedersen conductivity as well as the longitudinal gradient of the Pedersen conductivity weighted zonal wind plays the key role in determining the value of PRE. This is the same factor 1 mentioned in the discussion for the occurrence of irregularities in section 3.1. The flux tube integrated Pedersen conductivity in *E* region is affected by whether a synchronous sunset has occurred in the conjugate *E*-region ionospheres or not. Therefore, the magnetic declination angle plays a critical role in determining the magnitudes of the post sunset vertical drift velocities. Furthermore, the flux tube integrated *F*-region Pedersen conductivity depends on the ionospheric density level as well as the hemispheric density distribution in the conjugate ionospheres. Thus the largest variation should be seen during a solstice season. As the sunset terminator makes a large angle alignment with the magnetic flux tubes across the postsunset conjugate *E* regions at the longitude sectors of positive (plus signs) magnetic declination during the December solstice, the longitudinal gradient of the flux tube integrated Pedersen conductivities across the sunset terminator is greatly reduced so that the induced postsunset eastward electric field will be decreased. Similar situation will occur at the longitude sectors of negative (minus signs) magnetic declination during the June solstice season. Consequently, the resultant vertical drift velocity is reduced to almost nil as seen in Figure 2 in these regions of large magnetic declinations during the respective solstice season. Furthermore, the dip equator located with respect to the geographic equator that affects the ionospheric density level during a solstice season seems to offset some of the magnetic declination effect to either reduce or enhance the resultant vertical drift velocities. Specifically, the local winter ionospheric density level that occurred during the June solstice at longitudes 200–280° because it is located in the Southern Hemisphere seems to offset some of the positive (plus signs) magnetic declination effect to yield a smaller vertical drift velocities to indicate a decline trend in the vertical drift velocities in the positive zone in Figure 2. During the June solstice, an increasing trend of the vertical drift velocities that are observed at the negative magnetic declination zone of longitude 320–30° is located in the Northern Hemisphere is definitely caused by the local summer effect. For the case of December solstice, completely opposite trend of vertical drift variations is noted inside the longitude sector 140–280°, and inside the longitude sector 280–30°. Again this can be explained with the local seasonal effect of the ionospheric condition together with the magnetic declination effect at these particular longitude sectors during the December solstice season. Such seasonal variation of the ionospheric density level to affect the vertical drift velocity is similar to the effect of low or high solar activity that results in low or high vertical drift velocity.

[23] When the residual effect in the seasonal variation of the density distribution in relation to the magnetic declination during a solstice season is carried over to the following equinox season, the longitudinal variation of vertical drift velocities that are observed in the equinox season at longitude of large magnetic declination could somewhat resemble the longitudinal variation of vertical drift velocities that have occurred in the preceding solstice season at the same longitudes. It is thus speculated that the local winter effect that causes low vertical drift velocity observed during the December solstice at longitudes 120–200° where the magnetic declination is positive and is located in the Northern Hemisphere, has been carried over to the following March equinox to have smaller vertical drift velocities at these longitudes seen in Figure 2. On the

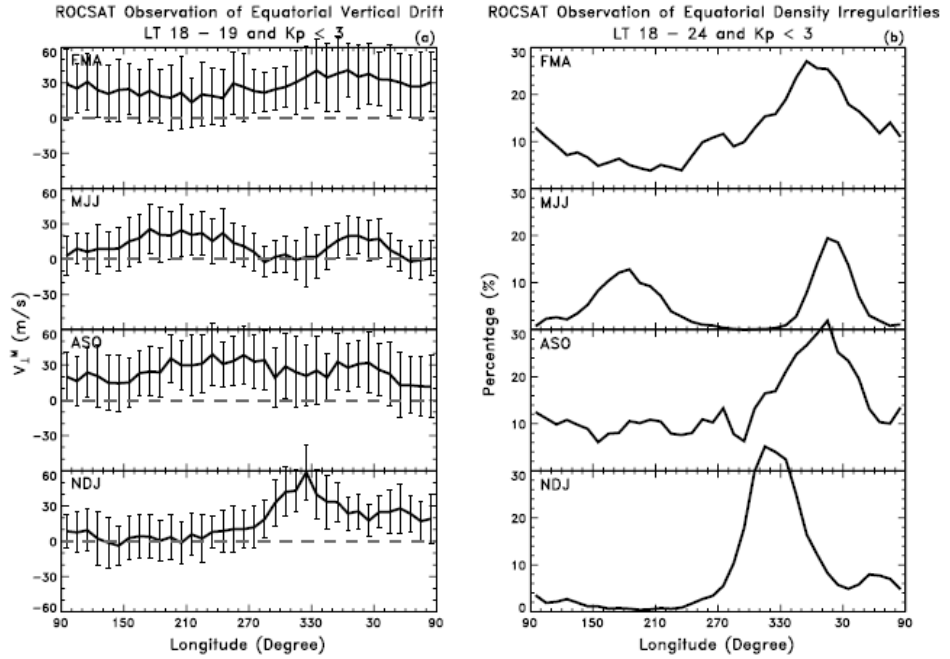

Figure 4. (a) Seasonal/longitudinal distributions of the ROCSAT observations of topside ionospheric vertical drift velocities copied from Figure 2. (b) Seasonal/longitudinal distributions of topside ionospheric irregularity occurrence rates observed by ROCSAT before midnight and during geomagnetic quiet period.

other hand, when the vertical drift velocity attains a higher value in the same longitude region during the June solstice in the northern summer season, some residual seasonal effect of the ionospheric density distribution seems to affect the following September equinox season to attain a slightly higher vertical drift velocity than in the March equinox season. Therefore, the vertical drift velocities at longitudes from 120 to 200° between the September equinox and the March equinox are different. Such residual seasonal effect seems to further include the longitude region up to 270° where the magnetic declination is positive as seen in Figure 2. Similar residual seasonal effect is also noticed for the contrasting seasonal variations of the vertical drift velocities during the two equinoxes at longitudes 320–30° of negative magnetic declination but are located in the Northern Hemisphere.

[24] Finally, the longitudinal variation of geomagnetic field strength at the dip equator can also affect the resultant vertical drift velocities. Because of the existence of the South Atlantic magnetic anomaly at longitudes around 300°, minimum field strength exists at the dip equator (about 22000 nT in comparison with the averaged value of 28000 nT) [cf. *Vichare and Richmond*, 2005] to yield a 20% higher vertical drift velocity around this longitude region. This could be one of the reasons for a higher vertical drift velocity noticed during the two equinox seasons around this longitude region in Figure 2, which then leads to higher occurrences of irregularities around this longitude region. The effect of the longitudinal variation of the magnetic field strength has been emphasized in the simulation study of the prereversal enhancement in a report of *Vichare and Richmond* [2005].

3.4. Correlation of Irregularity Occurrences With the Postsunset Vertical Drift Velocities

[25] With some understanding for the cause of the postsunset vertical drift velocities, we will study the correlation between the postsunset vertical drift velocity and the occurrence of density irregularities in the following. We would like to know if a longitude sector where the postsunset vertical drift velocity is always high on the average, the probability of observing a premidnight density irregularity occurrence will also be high in a statistical sense. Thus the equatorial density irregularity occurrences within ±15° in dip latitude during magnetic quiet times and within local time sectors 18–24 h is plotted in Figure 4b for comparison with the s/l distributions of vertical drift velocities replotted with the standard deviation in the 10° longitude bin in

Figure 4a. Here we would like to mention again that the data set used to derive the result in Figure 4a is different from the data set that yields the result of Figure 4b. The two data sets (ROCSAT orbits) are mutually exclusive from each other so that there is no sequential causal relationship existed between them within one ROCSAT orbital period of 96 min.

[26] By inspecting Figures 4a and 4b, we notice that similar gross features exist between the s/l distributions of the vertical drift velocities and the irregularity occurrence rates. This indicates that as the first approximation, the postsunset vertical drift is important to the occurrence of premidnight density irregularities as has been reported before [*Abdu et al.*, 1983, 2006; *Fejer et al.*, 1999]. However, we also notice that the two slightly different s/l distributions of vertical drift velocities during the March and September equinoxes have resulted in two similar distributions of irregularity occurrences for the two equinoxes.

[27] To better understand the relationship between the postsunset vertical drift velocities and the irregularity occurrences, a cross-correlation analysis between the vertical drift velocity in Figure 4a and the irregularity occurrence rate in Figure 4b for each season is carried out and the results are shown in Figure 5. Since the magnetic declination is an important factor in determining the postsunset vertical drift velocity, we use plus and minus signs in Figure 5 to identify data points taken at the two longitude zones of large magnetic declinations with reference to Figure 2. Data points from the near-zero magnetic declination zones are identified with circles in Figure 5.

[28] Different degrees of correlation are noted between the vertical drift velocity and the irregularity occurrence rate in different seasons. The best correlation occurs during the December solstice season and the worst one, in the September equinox. A couple of points can be concluded from the results in Figure 5. First, an ionosphere which always exhibits a large postsunset vertical drift velocity in a season seem to result in more frequent irregularity occurrences. This seems logical but is also less stringent than the conclusions made in the reports of *Abdu et al.* [1983, 2006] and *Fejer et al.* [1999], where a minimum threshold of the vertical drift velocity (about 10–15 m/s) is needed for the subsequent irregularity occurrences indicated in the former report; while in the latter report, this threshold of drift velocity to generate strong irregularities increases with solar activity. Again, it is emphasized that the current study is to correlate the s/l distributions of the postsuntset vertical drift velocities with the probability distribution in the s/l variations of irregularity occurrences in a statistical sense. No one-to-one causal relationship between the vertical drift velocity and the subsequent irregularity occurrence is provided here, as was studied by *Abdu et al.* [1983, 2006] or *Fejer et al.* [1999].

[29] Second, the cause of bad correlation between the vertical drift velocity and the irregularity occurrence during the September equinox seems to come from the fact that different longitudinal distributions of vertical drift velocities exist in the two equinoxes in contrast to the similar longitudinal distribution of irregularity occurrences in the two equinoxes, as was noted before. This can happen since the vertical drift velocity is caused mainly by factor 1 discussed in subsection 3.1; while the occurrence of postsunset irregularity comes from the combined effects of factors 1 and 2. Thus any seasonal variation of the neutral wind effect hidden in factor 2 such as the degree of hemispheric density asymmetry and the density level carried over from the previous solstice season can affect the instability growth of irregularity occurrences for the following equinox season even if the preconditioned postsunset vertical drift velocity from factor 1 has been set. A solar variability effect for the contrasting observations of irregularity occurrences has been made at longitudes of large magnetic declinations during a solstice season and is reported by *Su et al.* [2007]. Thus the postsunset vertical drift velocity seems to serve as one of the indicators in determining the irregularity occurrences in a season. It is thus claimed that the ionospheric condition such as the hemispheric distribution and density level serve as the additional supplements to the development of irregularity growth to complete the final s/l distributions. The instability initiating seed distribution could also be the additional factor, but it will be argued against this as shown in the next section 3.5.

[30] When the results of Figure 5 are further examined for each season, we notice that many data points with minus signs lie on the upper side (for higher irregularity occurrences) of the regression line to indicate that at longitudes of negative magnetic declination, higher occurrences of irregularities can come from a small vertical drift velocity. On the other hand, many larger vertical drift velocities (with plus signs) that fall below the fitted line also indicate failure of driving a large irregularity occurrence rate at longitudes of positive magnetic declination. This is most noticeable during the September equinox. All these data points that fall outside the fitted line seem to indicate that using the season as the reference in the correlation study between the vertical drift velocity and the irregularity occurrence may not be appropriate.

[31] Thus a new regression analysis is carried out using the longitude zones of different magnetic declinations as the reference to study the correlation between the vertical drift velocity and the irregularity occurrence. The results are plotted in Figure 6. We use the first letter of the season to identify the observation made in a season such as M for the March equinox, J for the June solstice and so on. From the fitted line in the regression analysis, we notice that the data points are scattered in such a way that there seems no seasonal differences. Two points can be concluded from Figure 6. First, the cross correlation between the vertical drift velocity and the irregularity occurrence rate is good in every longitude zone, and the proportionality constant between the two is about 15 m/s in the vertical drift velocity to have about 5–10% in irregularity occurrence probability. It should be noted that 5–10% probability of irregularity occurrence is rather high because the highest probability of irregularity occurrence per night is only about 30%. Thus when the postsunset vertical drift velocity is about 15 m/s, we can expect a 5–10% chance of observing an irregularity occurrence before midnight during a magnetic quiet time. Second, although the over-all correlation is improved, the correlation coefficient between the vertical drift velocity and the irregularity occurrence rate drop slightly in comparison with the better ones in the December solstice and March equinox shown in Figure 5. This implies that the effectiveness

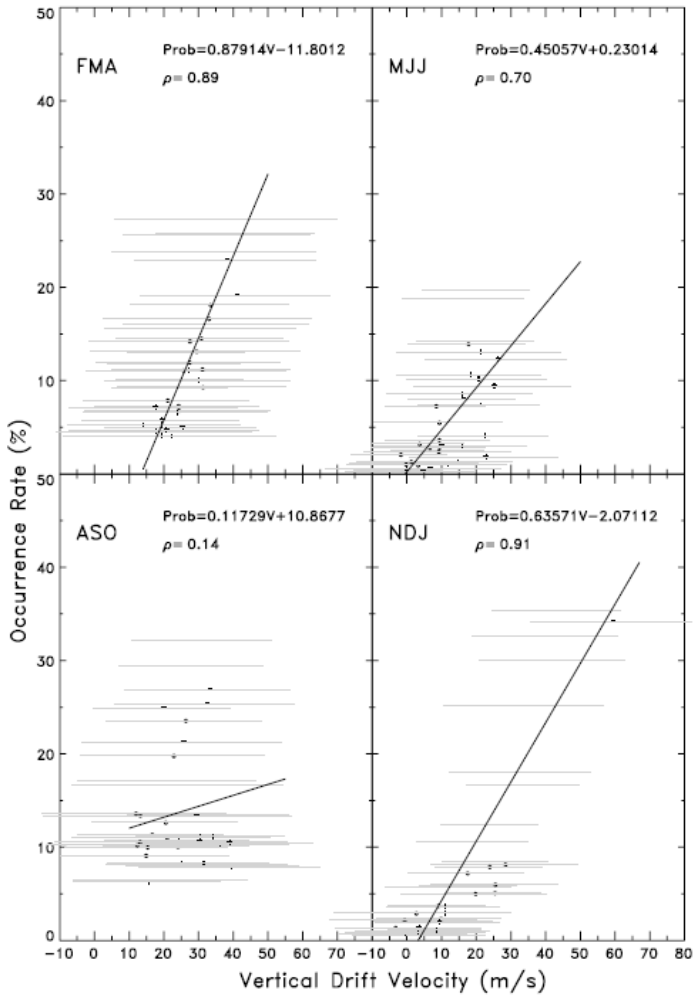

Figure 5. Linear regression analysis of the topside vertical drift velocities from Figure 4a with the irregularity occurrence rates from Figure 4b in each season. Data points labeled with plus and minus signs to identify data taken in the longitude regions of Figures 4a and 4b in which the magnetic declinations are positive and negative, respectively. Data points taken at longitudes of near-zero magnetic declination are labeled with circles.

of driving irregularity occurrence from vertical drift velocity could have some seasonal dependence. And this seasonal factor is the ionospheric density level and the hemispheric distribution that affects the growth of the irregularity as was mentioned before.

3.5. Seed Perturbations and Topside Irregularity Occurrences

[32] The importance of seed perturbation for the equatorial irregularity occurrences has been reported in many studies [e.g., *Rottger*, 1981; *Huang and Kelley*, 1996; *McClure et al.*, 1998; *Tsunoda*, 2005]. In the report of

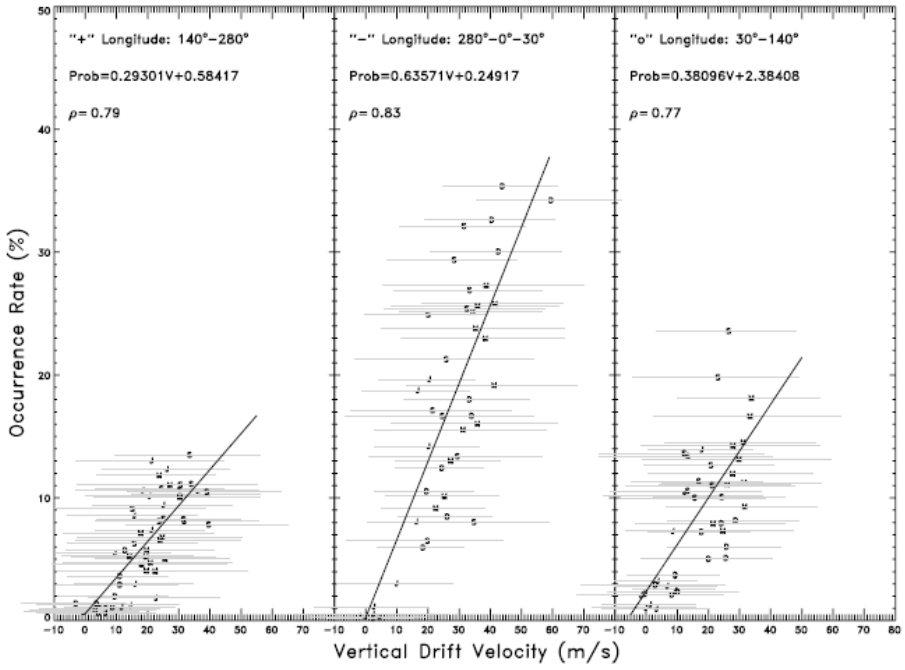

Figure 6. Linear regression analysis of the topside vertical drift velocities with irregularity occurrence rates at longitude regions with three different magnetic declinations. Data points are labeled with letters to identify the seasons of observations.

McClure et al. [1998], the authors claimed that the postsunset ionosphere seems to be always set in a favorable condition for the R-T instability process from the prereversal enhancement so that the final s/l distributions of irregularity occurrences should be related to the s/l distributions of seed perturbations. They further indicated that the s/l distributions of intertropical convergence zone (ITCZ) [*Waliser and Gautier*, 1993] correlate well with the s/l distributions of irregularity occurrences. The current study seems to indicate the other way around. We conclude that the s/l distributions of the postsunset vertical drift velocity are adequate to result in the observed s/l distributions of irregularity occurrences without adding any complementary s/l distributions of instability perturbation seeds from atmospheric disturbances. The s/l distributions of the postsunset vertical drift velocities have been shown to be controlled by the magnetic declinations for the seasonal variation in the alignment of the magnetic flux tube with respect to the sunset terminator and the seasonal variation of the background ionospheric condition at the dip equator of different geographic latitudes. The resultant s/l distributions of the equatorial density irregularities will also be controlled by these two effects. These two effects were first indicated by *Tsunoda* [1985] in studying the equatorial scintillation occurrences, and are now reconfirmed in this report. Furthermore, the geographic latitudinal effect of the seasonal variation in the background ionospheric condition at certain dip equator location is found to exceed the magnetic declination effect as seen in the following example.

[33] Using this example, we conclude that the longitudinal variations of the irregularity occurrences and the vertical drift velocities are related to the smooth global variation of the postsunset ionospheric condition from the smooth variations of the magnetic declination as well as slow seasonal variation effect in the ionosphere. There seems no need to add any other additional factors such as the atmospheric seed perturbations which could come from changes in the topographic feature across the longitudes to obtain the final s/l distributions of equatorial density irregularities. The illustrating example is carried out by comparing the results taken from a longitude region located between 250 and 280° in the eastern Pacific region where no topographic feature exists and the magnetic declination is positive against the result from a longitude region between 310 and 340° where the high Andes mountain range exists outside the western boundary of the region and the magnetic declination has a large negative value. Even with such contrasting topographic features and magnetic

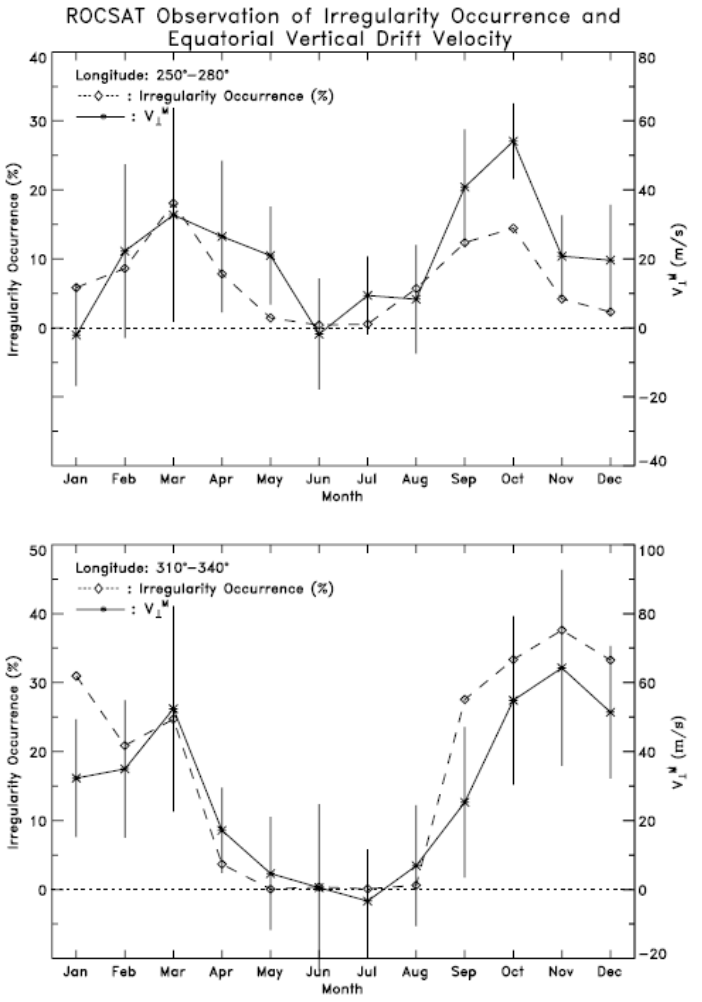

Figure 7. Comparison of the postsunset vertical drift velocities and the irregularity occurrences at two longitudes 250–280° and 310–340°.

declinations, the irregularity occurrence rates as well as the vertical drift velocities are very similar to each other in the monthly variation as shown in Figure 7. We could have used a longitude sector 290–320°, or 300–330° to illustrate the topographic contrast to the longitudes 250–280°, but we adopt the longitude sector 310–340° to avoid any spill-over effect from the close proximity to the longitudes 250–280°, when the smooth variations of the verticals drift velocities as well as the irregularity occurrences between two longitude regions is the point of discussion.

[34] The result at longitudes 310–340° shown in the lower section of Figure 7 is discussed first. We noticed that the monthly variation of vertical drift velocities tracks very closely to that of irregularity occurrence rates. This seems to indicate that the vertical drift velocity can drive the final irregularity occurrence in good proportion. Furthermore, extremely low irregularity occurrence rates are observed

during the June solstice, and very high irregularity occurrences exist during the December solstice as well as in the two equinox seasons. The opposite behavior in both the vertical drift velocity and the irregularity occurrence for the two solstice seasons can be easily understood from the existence of a large negative magnetic declination in these longitude regions. Such drastic variation in the monthly irregularity occurrence distribution has also been reported before with ionosonde data taken at Fortaleza station (longitude 321.55°) in the Brazilian sector [*Abdu et al.*, 1992].

[35] As for the longitude sector 250–280° seen in the upper section of Figure 7, again the monthly variation of the vertical drift velocities tracks pretty close to that of irregularity occurrences. However, a lesser degree of correlation is noted between the two than what is observed at longitudes 310–340°. Furthermore, these longitude regions have positive magnetic declinations, yet the vertical drift velocity as well as the irregularity occurrence rate is observed to have a minimum during the June solstice, and the maxima during the two equinoxes. Such result has been noticed before in the 1.54 GHz amplitude scintillation experiments carried out at the Huancayo station (longitude 283°) where the equinoctial maximum and the June solstice minimum have been observed [*Basu et al.*, 1980]. The minimum occurrence during the June solstice seems to be resulted from the local winter effect in the ionospheric conditions at longitudes 250–280° that are located in the Southern Hemisphere. The effect of positive magnetic declination at longitudes 250–280° seem to have been offset by the low density level on the postsunset ionosphere existed during the local winter in the June solstice. On the other hand, the positive magnetic declination effect prevails during the December solstice season to indicate low occurrence rates for both vertical drift velocities and irregularity occurrences.

[36] The similarities of the observations made at longitudes 250–280° and 310–340° in Figure 7 are highlighted by the low occurrences of both the vertical drift velocities and the irregularity occurrences during the June solstice in these two longitude regions. The cause can be explained by the continuing and slow variation of the ionospheric conditions from the magnetic declination effect together with the local seasonal effect at the dip equator. The effect of perturbation seeds that could come from the change of the topographic feature in the Andes mountain range and the pattern variation in the ITCZ is not apparent in the monthly variations of vertical drift velocities and irregularity occurrences between these two longitude regions. Therefore, it implies that the postsunset vertical drift velocity can serve as the final indicator to determine the statistical outcome of the equatorial density irregularity occurrence probability without any additional topographic related gravity wave seeding. In other words, as we expand the conclusion made by *Mendillo et al.* [2001] that the electrodynamic $E \times B$ effect in the postsunset ionosphere is the most important factor in deciding the irregularity occurrence to further include the postsunset ionospheric background condition as the other supplementary factor, then the observed s/l distributions of irregularity occurrences need no additional instability triggering seed distribution to complete the final s/l distributions of irregularity occurrences. Such de-emphasis of the importance of the perturbation seeds from atmospheric disturbances can also be inferred from the extensive studies of bottom-type layers as the precursors of large-scale radar plumes observed by JULIA radar reported by *Hysell and Burcham* [1998] and *Hysell* [2000]. The omnipresences of bottom-type layers during nights of equinox season do not necessarily come from the atmospheric seed perturbations, but can be controlled by the evening vortex in the postsunset *F*-region ionosphere in which large-scale wave structure can be formed [cf. *Haerendel et al.*, 1992; *Eccles et al.*, 1999; *Kudeki and Bhattacharyya*, 1999; *Tsunoda*, 2005].

4. Conclusions

[37] The global temporal/spatial variations of density irregularity occurrence rate has been obtained with the ROCSAT data taken during high to moderate solar activity years of 1999–2004. The current result provides a good reference for the global monthly/seasonal/longitudinal distributions of irregularity occurrence pattern to fill the gap in some eastern Pacific regions from past observations. The result further indicates that the monthly occurrence variation changes gradually and smoothly in the occurrence pattern across the longitudes. This is attributed to the fact that the cause of irregularity occurrence is most importantly related to the high-postsunset ionosphere resulted from the induced eastward electric field that is closely related to the magnetic declination. In addition, the seasonal variation of the background ionospheric condition at the location of the dip equator with respect to the geographic equator also contributes to a smooth variation of irregularity occurrences across the longitudes. Such smooth variation in the postsunset vertical drift velocities as well as the irregularity occurrences is illustrated with the comparison of the results taken from two separate longitude sectors 250–280° and 310–340°, where opposite topographic feature and magnetic declination exist. It is thus concluded that the instability seeding perturbations from atmospheric disturbances can be ignored in the final s/l distributions of irregularity occurrences at the topside ionosphere. Although we have no theoretical model calculation to back it up, we feel our conclusion points to the right direction because the instability perturbation seeds from atmospheric disturbances fail to show any role in the current statistical study in determining the final monthly/seasonal/longitudinal distributions of vertical drift velocities as well as irregularity occurrences. One thing that needs to be studied in the future is the solar variability effect in the monthly/seasonal/longitudinal distributions of vertical drift velocities and irregularity occurrences, and their relationship to each other during a fixed solar activity period. This will be done when more space observations become available.

[38] **Acknowledgments.** The work was supported in part by NSC96-2111-M-008-005 from the National Science Council of the Republic of China, and in part by a grant from the Asian Office of Aerospace Research and Development (AOARD) of the U. S. Air Force Office of Scientific Research (AFOSR) (AOARD-06-4046 and AOARD-07-4098). The ROCSAT data is processed under the grant 93-NSPO(B)-IPEI-FA07-01 from the National Space Organization of the Republic of China. We are grateful to many NCU ROCSAT/IPEI team members for their efforts in processing the ROCSAT/IPEI data. We also acknowledge the reviewers' comments that lead to some new findings from the results in Figure 2.

[39] Amitava Bhattacharjee thanks Paluri Rama Rao and another reviewer for their assistance in evaluating this manuscript.

References

Aarons, J. (1977), Equatorial scintillations: A review, *IEEE Trans. Antennas Propag.*, *25*, 729–736, doi:10.1109/TAP.1977.1141649.

Aarons, J. (1982), Global morphology of ionospheric scintillation, *Proc. IEEE*, *70*, 360–378.

Aarons, J. (1993), The longitudinal morphology of equatorial *F*-layer irregularities relevant to their occurrence, *Space Sci. Rev.*, *63*, 209–243, doi:10.1007/BF00750769.

Abdu, M. A., J. A. Bittencourt, and I. S. Batista (1981), Magnetic declination control of the equatorial *F* region dynamo electric field development and spread *F*, *J. Geophys. Res.*, *86*, 11,443–11,446, doi:10.1029/JA086iA13p11443.

Abdu, M. A., R. T. deMedieros, and J. H. L. Sobral (1982), Equatorial spread *F* instability conditions as determined from ionogram, *Geophys. Res. Lett.*, *9*, 692–695, doi:10.1029/GL009i006p00692.

Abdu, M. A., R. T. Medeiros, J. A. Bittencourt, and I. S. Batista (1983), Vertical ionization drift velocities and range type spread *F* in the evening equatorial ionosphere, *J. Geophys. Res.*, *88*, 399–402, doi:10.1029/JA088iA01p00399.

Abdu, M. A., I. S. Batista, and J. H. A. Sobral (1992), A new aspect of magnetic declination control of equatorial spread *F* and *F* region dynamo, *J. Geophys. Res.*, *97*, 14,897–14,904, doi:10.1029/92JA00826.

Abdu, M. A., K. N. Iyer, R. T. de Medeiros, I. S. Batista, and J. H. A. Sobral (2006), Thermospheric meridional wind control of equatorial spread *F* and evening prereversal electric field, *Geophys. Res. Lett.*, *33*, L07106, doi:10.1029/2005GL024835.

Basu, S., and S. Basu (1985), Equatorial scintillations: Advances since ISEA-6, *J. Atmos. Terr. Phys.*, *47*, 753–768, doi:10.1016/0021-9169(85)90052-2.

Basu, S., S. Basu, and B. K. Khan (1976), Model of equatorial scintillation from in-situ measurements, *Radio Sci.*, *11*, 821–832, doi:10.1029/RS011i010p00821.

Basu, S., S. Basu, J. P. Mullen, and A. Bushby (1980), Long-term 1.5 GHz atmplitude scintillation measurements at magnetic equator, *J. Geophys. Res.*, *7*, 259–262.

Batista, I. S., M. A. Abdu, and J. A. Bittencourt (1986), Equatorial *F* region vertical plasma drifts: Seasonal and longitudinal asymmetries in the American sector, *J. Geophys. Res.*, *91*(A11), 12,055–12,064, doi:10.1029/JA091iA11p12055.

Bowman, G. G. (1984), A comparison of mid-latitude and equatorial-latitude spread-*F* characteristics, *J. Atmos. Terr. Phys.*, *46*, 65–71, doi:10.1016/0021-9169(84)90045-X.

Crain, D. J., R. A. Heelis, G. J. Bailey, and A. D. Richmond (1993), Low-latitude plasma drifts from a simulation of the global atmospheric dynamo, *J. Geophys. Res.*, *98*, 6039–6046, doi:10.1029/92JA02196.

Eccles, J. V. (1998a), A simple model of low-latitude electric fields, *J. Geophys. Res.*, *103*, 26,699–26,708, doi:10.1029/98JA02657.

Eccles, J. V. (1998b), Modeling investigation of the evening prereversal enhancement of the zonal electric field in the equatorial ionosphere, *J. Geophys. Res.*, *103*, 26,709–26,719.

Eccles, J. V., N. Maynard, and G. Wilson (1999), Study of the evening plasma drift vortex in the low-latitude ionosphere using San Marco electric field measurements, *J. Geophys. Res.*, *104*, 28,133–28,143, doi:10.1029/1999JA900373.

Farley, D. T., B. B. Balsley, R. F. Woodman, and J. F. McClure (1970), Equatorial spread *F*: Implications of VHF radar observations, *J. Geophys. Res.*, *75*, 7199–7216, doi:10.1029/JA075i034p07199.

Fejer, B. G., E. R. de Paula, R. A. Heelis, and W. B. Hanson (1995), Global equatorial ionospheric vertical drifts measured by AE-E satellite, *J. Geophys. Res.*, *100*, 5769–5776, doi:10.1029/94JA03240.

Fejer, B. G., L. Scherliess, and E. R. de Paula (1999), Effects of the vertical plasma drift velocity on the generation and evolution of equatorial spread *F*, *J. Geophys. Res.*, *104*, 19,859–19,869, doi:10.1029/1999JA900271.

Fejer, B. G., J. W. Jensen, and S.-Y. Su (2008), Quiet time equatorial *F* region vertical plasma drift model derived from ROCSAT-1 observations, *J. Geophys. Res.*, doi:10.1029/2007JA012801, in press.

Fesen, C. G., G. Crowley, R. G. Roble, A. D. Richmond, and B. G. Fejer (2000), Simulation of the pre-reversal enhancement in the low latitude vertical ion drifts, *Geophys. Res. Lett.*, *27*, 1851–1854, doi:10.1029/2000GL000061.

Haerendel, G., J. V. Eccles, and S. Cakir (1992), Theory for modeling the equatorial evening ionosphere and the origin of the shear in the horizontal plasma flow, *J. Geophys. Res.*, *97*, 1209–1223, doi:10.1029/91JA02226.

Heelis, R. A., P. C. Kendall, R. J. Moffett, D. W. Windle, and H. Rishbeth (1974), Electrical coupling of the *E*- and *F*- regions and its effect on *F*-region drifts and winds, *Planet. Space Sci.*, *22*, 743–756, doi:10.1016/0032-0633(74)90144-5.

Hei, M. A., R. A. Heelis, and J. P. McClure (2005), Seasonal and longitudinal variation of large-scale topside equatorial plasma depletions, *J. Geophys. Res.*, *110*, A12315, doi:10.1029/2005JA011153.

Huang, C.-S., and M. C. Kelley (1996), Nonlinear evolution of equatorial spread *F*: 4. Gravity waves, velocity shear, and day-to-day variability, *J. Geophys. Res.*, *101*, 24,521–24,532, doi:10.1029/96JA02332.

Huang, C. Y., W. J. Burke, J. S. Machuzak, L. C. Gentile, and P. J. Sultan (2002), Equatorial plasma bubbles observed by DMSP satellite during a full solar cycle: Toward a global climatology, *J. Geophys. Res.*, *107*(A12), 1434, doi:10.1029/2002JA009452.

Hysell, D. (2000), An overview and synthesis of plasma irregularities in equatorial spread *F*, *J. Atmos. Sol. Terr. Phys.*, *62*, 1037–1056, doi:10.1016/S1364-6826(00)00095-X.

Hysell, D. L., and J. D. Burcham (1998), JULIA radar studies of equatorial spread *F*, *J. Geophys. Res.*, *103*, 29,155–29,167, doi:10.1029/98JA02655.

Kil, H., and R. A. Heelis (1998), Global distribution of density irreularites in the equatorial ionosphere, *J. Geophys. Res.*, *103*, 407–417, doi:10.1029/97JA02698.

Kudeki, E., and S. Bhattacharyya (1999), Postsunset votex in the equatorial *F*-region plasma and implications for bottomside spread-*F*, *J. Geophys. Res.*, *104*, 28,163–28,170, doi:10.1029/1998JA900111.

Maruyama, T. (1988), A diagnostic model for equatorial spread *F*: 1. Model description and application to electric field and neutral wind effects, *J. Geophys. Res.*, *93*, 14,611–14,622, doi:10.1029/JA093iA12p14611.

Maruyama, T., and N. Matuura (1980), Global distribution of occurrence probability of spread echoes based on ISS-b observation, *J. Radio Res. Lab. Jpn.*, *27*, 201–216.

Maruyama, T., and N. Matuura (1984), Longitudinal variability of annual changes in activity of equatorial spread-*F* and plasma bubbles, *J. Geophys. Res.*, *89*, 10,903–10,912, doi:10.1029/JA089iA12p10903.

McClure, J. P., S. Singh, D. K. Bamgboye, F. S. Johnson, and H. Kil (1998), Occurrence of equatorial *F* region irregularities: Evidence for tropospheric seeding, *J. Geophys. Res.*, *103*, 29,119–29,135, doi:10.1029/98JA02749.

Mendillo, M., J. Meriwether, and M. Biondi (2001), Testing the thermospheric neutral wind suppression mechanism for day-to-day variability of equatorial spread *F*, *J. Geophys. Res.*, *106*(A3), 3655–3663, doi:10.1029/2000JA000148.

Ossakow, S. L. (1981), Spread *F* theories—A review, *J. Atmos. Terr. Phys.*, *43*, 437–452, doi:10.1016/0021-9169(81)90107-0.

Ossakow, S. L., S. T. Zalesak, B. E. McDonald, and P. K. Chaturvedi (1979), Nolinear equatorial spread *F*: Dependence on altitude of the *F* peak and bottomside electron density gradient length, *J. Geophys. Res.*, *84*, 17–29, doi:10.1029/JA084iA01p00017.

Rastogi, R. M. (1980), Seasonal and solar cycle variation of equatorial spread *F* in the American sector, *J. Atmos. Terr. Phys.*, *42*, 593–597, doi:10.1016/0021-9169(80)90093-8.

Rishbeth, H. (1971), Polarization fields produced by winds in the ionospheric *F*-region, *Planet. Space Sci.*, *19*, 357–369, doi:10.1016/0032-0633(71)90098-5.

Rishbeth, H. (1977), Dynamics of equatorial *F*-region, *J. Atmos. Terr. Phys.*, *39*, 1159–1168, doi:10.1016/0021-9169(77)90024-1.

Rishbeth, H. (1981), The *F*-region dynamo, *J. Atmos. Terr. Phys.*, *43*, 387–392, doi:10.1016/0021-9169(81)90102-1.

Rottger, J. (1981), Equatorial spread-*F* by electric fields and atmospheric gravity waves generated by thunderstorms, *J. Atmos. Terr. Phys.*, *43*, 453–462, doi:10.1016/0021-9169(81)90108-2.

Stolle, C., H. Luehr, M. Rother, and G. Balasis (2006), Magnetic signatures of equatorial spread-*F* as observed by the CHAMP satellite, *J. Geophys. Res.*, *111*, A02304, doi:10.1029/2005JA011184.

Su, S.-Y., C. H. Liu, H. H. Ho, and C. K. Chao (2006), Distribution characteristics of topside ionospheric density irregularities: Equatorial regions versus midlatitudes, *J. Geophys. Res.*, *111*, A06305, doi:10.1029/2005JA011330.

Su, S.-Y., C. K. Chao, C. H. Liu, and H. H. Ho (2007), Meridional wind effect on anti-solar activity correlation of equatorial density irregularity distribution, *J. Geophys. Res.*, *112*, A10305, doi:10.1029/2007JA012261.

Sultan, P. J. (1996), Linear theory and modelling of the Rayleigh-Taylor instability leading to the occurrence of equatorial spread *F*, *J. Geophys. Res.*, *101*, 26,875–26,891, doi:10.1029/96JA00682.

Tsunoda, R. T. (1985), Control of the seasonal and longitudinal occurrence of equatorial scintillations by the longitudinal gradient in integrated *E* region Pedersen conductivity, *J. Geophys. Res.*, *90*, 447–456, doi:10.1029/JA090iA01p00447.

Tsunoda, R. T. (2005), On the enigma of day-to-day variability in equatorial spread *F*, *Geophys. Res. Lett.*, *32*, L08103, doi:10.1029/2005GL022512.

Vichare, G., and A. D. Richmond (2005), Simulation study of the longitudinal variation of evening vertical ionospheric drifts at the magnetic equator during equinox, *J. Geophys. Res.*, *110*, A05304, doi:10.1029/2004JA010720.

Waliser, D. E., and C. Gautier (1993), A satellite derived climatology of the ITCZ, *J. Clim.*, *6*, 2162–2174, doi:10.1175/1520-0442(1993)006<2162:ASDCOT>2.0.CO;2.

Watanabe, S., and H. Oya (1986), Occurrence characteristics of low latitude ionospheric irregularities observed by impedance probe on board the Hinotori satellite, *J. Geomagn. Geoelectr.*, *38*, 125–149.

Zalesak, S. T., and S. L. Ossakow (1980), Nonlinear equatorial spread *F*: Spatially large bubbles resulting from large horizontal scale initial perturbations, *J. Geophys. Res.*, *85*, 2131–2142, doi:10.1029/JA085iA05p02131.

C. K. Chao, Institute of Space Science, National Central University, Chung-Li, 320, Taiwan.

C. H. Liu, Academia Sinica, 128 Academia Road, Section 2, Nankang, Taipei 115, Taiwan.

S.-Y. Su, Institute of Space Science and Center for Space and Remote Sensing Research, National Central University, Chung-Li, 320, Taiwan. (sysu@jupiter.ss.ncu.edu.tw)